Supplement to

"Grounding line migration through the calving season of Jakobshavn Isbræ, Greenland, observed with terrestrial radar interferometry"

Surui Xie[1], Timothy H. Dixon[1], Denis Voytenko[2], Fanghui Deng[1], David M. Holland[2,3]

1. School of Geosciences, University of South Florida, Tampa, FL, USA

2. Courant Institute of Mathematical Sciences, New York University, New York, NY, USA

3. Center for Global Sea Level Change, New York University, Abu Dhabi, UAE

Correspondence: Surui Xie <suruixie@mail.usf.edu>

Contents:

Text S1: Method to fix phase offsets in the 2012 data

Text S2: PSD plots for 2012 and 2015

Text S3: Tide and tidal rate

Text S4: Step-change in the mélange of 2016

Text S5: Phase lag maps for K1 and S2 tidal frequencies

Text S6: Movies shown major calving event during 3 campaigns

Figure and movie contents are introduced in the text.

1. Method to fix phase offsets in the 2012 data

The ice velocity estimates have some significant offsets in the 2012 data. These offsets represent phase discontinuities, clustering at integer multiples of the radar wavelength (Fig S1(a)). They occur because the 2012 data were acquired with a scan rate that was slow compared to ice velocity, such that ice could move more than one radar wavelength during the 3 minute scan interval (data in later years were acquired with a faster scan rate). Compared to fast moving ice, rocks near the TRI can be treated as stationary objects. We used a rock reference point ~0.2 km away from the radar as a reference for phase unwrapping. To correct the phase discontinuities caused by phase unwrapping error, we first used a model to fix the phase offsets for a single point on ice (P0, yellow point in Fig S1(b)), then used it as reference point for phase unwrapping to get velocity maps relative to this point. Ice velocities relative to the stationary rock were then generated by adding the modeled velocities of P0 to those relative velocities. We selected data obtained between 6 August and 10 August for the following process because there were continuous measurements during this period and only one small calving event. Here are the 4 steps used to model the velocity of P0:

1) Use the same data processing procedure as described in *Voytenko et al.* [2015)] and *Xie et al.* [2016], generating time series for all velocity maps. The generated velocities are absolute velocities, plus/minus some value equal to an integer number of wavelength jumps. The TRI instrument transmits Ku-band microwaves with wavelength of 1.74 cm. In a 2-way measurement system, 1 wavelength jump in unwrapped phase leads to 0.87 cm

change in the LOS displacement, equal to 4.2 m d^{-1} offset in LOS velocity when the repeating time of measurement is 3 minutes. From Fig S1(a) we infer that most of the unwrapped phases for P0 have 4 cycles of phase offset.

2) Remove "apparent outliers" by using the modified Z-score method [*Iglewicz and Hoaglin,* 1993]. For the *i*th observation x_i, its Z-score is:

$$Z_i = 0.6745(x_i - \tilde{x}) / \text{MAD} \quad \text{(S1)}$$

where MAD denotes the median absolute deviation, and $\tilde{x}$ is the median value. Observations with absolute value of the modified Z-scores >3.5 were considered as outliers and removed. Then we subtracted a 2nd-order polynomial curve to remove the possible response to calving events. The method by *Davis et al.* [2014] was then used to estimate the periodic components caused by tidal variations. We chose 3 sinusoids with the same frequencies as the K1/M2/S2 tidal constituents (see the main paper for more information about the tidal constituents at Jakobshavn Isbræ). The solid blue curve in Fig S1(c) shows the best fit of a 2nd-order polynomial + 3 sinusoids to the observed time series. The dashed blue curves mark 3 times the value of the root-mean-square (RMS) of the residuals.

3) Shift all observations (including "apparent outliers" in step 2) upwards/downwards by 4.2×N m d^{-1}, where N = 0, ±1, ±2, ±3, ±4, ±5, etc. Observations who's shifted values do not fall into the 3×RMS space defined in step 2 are labeled as outliers (grey dots in Fig S1(c)) and removed. Values that fall within the 3×RMS space are then shifted by 4 cycles of phase offset (16.8 m d^{-1}) to eliminate the jumps derived by feature tracking method in step 1.

4) Apply a median filter (kernel size = 3) to the time series from step 3, and then use the same model in step 2 to fit the new time series. Estimated parameters are then used for further processing. Fig S1(d) shows the least square fit of the final fixed time series for P0.

For all other points on the TRI image, their velocities are estimated by adding the modeled velocity of P0 to their relative velocities. Fig S2 shows phase offsets-fixed LOS velocities for selected points. Black dots are velocity estimates when using a stationary rock point as the reference point for phase unwrapping (shifted upwards by 4 cycles of phase offsets). From Fig S2 we see that phase jumps are greatly reduced by this method, especially on the glacier. In the mélange, time series shortly after two calving events (on 5 August and 9 August, see blue arrows in Fig S1(a)) still have some jumps, mainly due to phase breaks caused by rapid ice motion after calving events. In the tidal analysis section of the main paper, we omit data for the mélange acquired near these 2 calving events.

We used feature tracking (done with OpenCV: http://opencv.org/) as an independent method to examine the phase offset "fixed" velocities from interferometry. Fig S3(a) is the median LOS velocity map from a 1 day sequential measurements in the 2012 campaign. Fig S3(b) shows a velocity map (projected onto the LOS direction) derived by feature tracking using two TRI intensity images acquired at the beginning and end of the day (red means moving towards the radar, green means moving away). Fig S3(c) is the difference between (a) and (b). Red means the velocity estimated by interferometry is larger than the velocity estimated by feature tracking, green means it is less. For most points, the difference is much smaller than 1 cycle of

phase jump (4.2 m d^{-1}). On the north edge of the mélange, there is a small area where offsets still exist, presumably caused by phase breaks due to discontinuities in the TRI maps. One way to solve this type of phase jump is to use shorter repeat time when collecting data. However, this problem won't affect the following tidal analysis if the sign of LOS velocity has not been changed by these phase jumps. Because this study focuses on short time-scale tidal responses, the large background velocity was detrended before tidal analysis. We also noticed that the velocity differences near the radar are much larger, up to a few cycles of phase jumps. This is due to the fact that the phase data for stationary areas near the radar have no discontinuity problems as on the ice. The method described above has thus introduced some artificial jumps in the stationary near field.

Fig S4 and S5 show comparisons of velocity estimates by interferometry and feature tracking for 2015 and 2016. There are no systematic differences for these two years. Except for some random errors, significant difference only appear in isolated patches where the phase map lacks continuity, or in places close to where calving events have occurred. Thus, we did not apply the same method used for 2012 to the 2015 and 2016 data. Instead, we did phase unwrapping by using stationary points on rocks only.

2. PSD plots for 2012 and 2015

Fig S6, power spectral density (PSD) for selected areas in 2012

Fig S7, power spectral density (PSD) for selected areas in 2015

3. Tide and tidal rate

In this study, tidal rate is defined as the 1st time derivative of tidal height. For a tide signal:

$$H(t) = A\cos(2\pi ft + \varphi) \tag{S2}$$

where A is the amplitude, f is the frequency, φ is the phase. The tidal rate is:

$$H'(t) = 2\pi fA\cos(2\pi ft + \varphi + 0.5\pi) \tag{S3}$$

Compare to tidal height, the amplitude of tidal rate has been amplified by $2\pi f$. Due to differentiation, the phase difference between ice velocity and tidal rate is the same as the phase difference between ice position and tidal height.

4. Step-change in the mélange of 2016

A one day of TRI measurements from 2016 was used to obtain a median average DEM for the terminus region. This DEM shows a step-change in ice elevation in the mélange. The step is located in the approximate position of the ice front in summer 2005, and might represent a submarine end moraine. Alternately, it represents a pressure ridge ("ice arch") associated with congested ice flow in the fjord. To estimate the average elevation difference, we cropped two representative 1.2 km × 0.8 km areas (dashed boxes in Fig S8(b)), and used the median height in each area to represent the respective height in the two areas. Height difference was estimated at 10 m, larger than the height uncertainty, 2–3 m [*Strozzi et al.*, 2012; *Xie et al.*,

2016]. We also estimated the height of the largest nearby iceberg (marked by yellow arrow in Fig S8(b)), which is ~60 m above local sea level. Assuming 917 kg m^{-3} for ice density, and 1000 kg m^{-3} for water density, and assuming the ice column is in buoyancy-gravity equilibrium, the 60 m high iceberg has ~660 thickness below water line. This is smaller than the ~730 m water depth at the iceberg location using the bathymetry model of *An et al.* [2017], implying that bottom topography should not influence mélange topography. However, available bathymetry models have low resolution (a few hundred m), and narrow topographic features such as an underwater moraine could be missed.

Except for the elevation change, both TRI intensity images and satellite optical images (Fig S9) show that there is significant difference in surface roughness across the step-change. We use a horizontal plane to fit the outlined area in Fig S8(b) on each side of the step-change, and use the RMS of elevation difference to represent the surface roughness. Ice upstream from the step-change (dashed red box in Fig S8(b)) has a roughness of 5 m, while ice downstream (dashed blue box in Fig S8(b)) has a roughness of 2 m. If the step-change is caused by a submarine topographic obstruction it could act as a "filter", such that only smaller icebergs can pass, contributing to the difference in surface roughness. A narrowing of the fjord's horizontal dimensions could also affect roughness on each side of the step-change, holding back large new icebergs, and allowing surface melting to decrease the height of older icebergs downstream from the step.

The step-change was not visually distinct in the first 3 days of the 2016 campaign. Following

that, several calving events at the glacier front as well as calving-like events in the mélange made it visually obvious (watch Mov S3). We suspect that mélange ice upstream from the step-change was compressed by a sequence of rapid calving events, which could magnify this elevation difference. If this is correct, the response of mélange to tidal variation could differ upstream and downstream from the step-change. Unfortunately, ice velocity time series are very noisy downstream from the step-change place, and it is difficult to determine the difference in tidal responses (Fig S8). However, for ice in the mélange, the relatively stable ice motion upstream from the step-change zone, and the very irregular ice velocity downstream, suggests that ice upstream of the step is much stiffer than ice downstream.

5. Phase lag maps for K1 and S2 tidal frequencies

Fig S10, phase lag in time (h) for K1 and S2 tidal frequencies.

6. Movies shown major calving event during 3 campaigns

Mov S1, Major calving events in 2012.

Mov S2, Major calving events in 2015.

Mov S3, Major calving events in 2016.

References

An, L., Rignot, E., Elieff, S., Morlighem, M., Millan, R., Mouginot, J., Holland, D.M., Holland, D. and Paden, J.: Bed elevation of Jakobshavn Isbræ, West Greenland, from high-resolution airborne gravity and other data, Geophys. Res. Lett., 44(8), 3728–3736, doi: 10.1002/2017GL073245, 2017.

Davis, J.L., De Juan, J., Nettles, M., Elosegui, P. and Andersen, M.L.: Evidence for non-tidal diurnal velocity variations of Helheim Glacier, 15 East Greenland, J. Glaciol., 60(224), 1169–1180, doi:10.3189/2014JoG13J230, 2014.

Iglewicz, B. and Hoaglin, D.C.: How to detect and handle outliers (Vol. 16), Asq Press, 1993.

Lomb, N.R.: Least-squares frequency analysis of unequally spaced data, Astrophysics and space science, 39(2), 447–462, doi:10.1007/BF00648343, 1976.

Scargle, J.D.: Studies in astronomical time series analysis, II-Statistical aspects of spectral analysis of unevenly spaced data, The Astrophys- ical Journal, 263, 835–853, doi: 10.1086/160554, 1982.

Strozzi, T., Werner, C., Wiesmann, A. and Wegmuller, U.: Topography mapping with a portable real-aperture radar interferometer, IEEE Geosci. Remote Sens. Lett., 9(2), 277–281, doi: 10.1109/LGRS.2011.2166751, 2012.

Voytenko, D., Dixon, T.H., Howat, I.M., Gourmelen, N., Lembke, C., Werner, C.L., De La Peña, S. and Oddsson, B.: Multi-year observations of Breiðamerkurjökull, a marine-terminating glacier in southeastern Iceland, using terrestrial radar interferometry, J. Glaciol., 61(225), 42–54, doi:10.3189/2015JoG14J099, 2015.

Xie, S., Dixon, T.H., Voytenko, D., Holland, D.M., Holland, D. and Zheng, T.: Precursor motion to iceberg calving at Jakobshavn Isbræ, Greenland, observed with terrestrial radar interferometry, J. Glaciol., 62(236), 1134–1142, doi:10.1017/jog.2016.104, 2016.

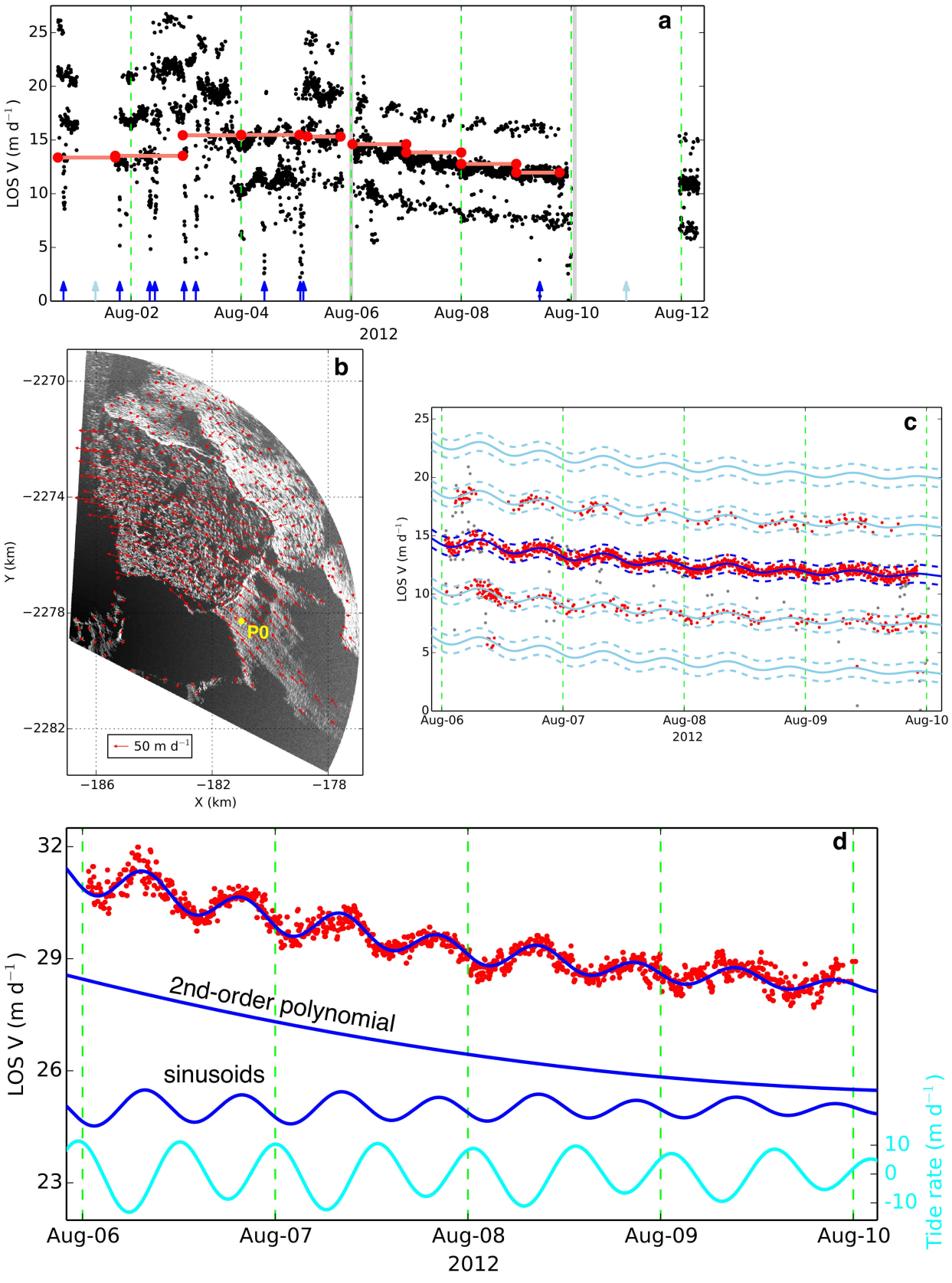
a
LOS V (m d^{-1})
0
5
10
15
20
25
Aug-02
Aug-04
Aug-06
Aug-08
Aug-10
Aug-12
2012
b
Y (km)
−2270
−2274
−2278
−2282
P0
50 m d^{-1}
−186
−182
−178
X (km)
c
LOS V (m d^{-1})
0
5
10
15
20
25
Aug-06
Aug-07
Aug-08
Aug-09
Aug-10
2012
d
LOS V (m d^{-1})
23
26
29
32
2nd-order polynomial
sinusoids
10
0
-10
Tide rate (m d^{-1})
Aug-06
Aug-07
Aug-08
Aug-09
Aug-10
2012

Figure S1. (**a**), LOS velocity time series (black dots) of P0 on (b), when using a stationary point on rock as reference for phase unwrapping. Salmon bars show velocities by feature tracking method (shifted downwards by phase jumps of 4 cycles of radar wavelength), separated by ~1 d. Blue arrows mark visible calving events on TRI intensity images, two light blue arrows represent calving events that were in observation gaps. (**b**), Point (P0) chosen as reference point for phase unwrapping to estimate relative velocities. Red arrows show 2-D velocity map by tracking two TRI intensity images between 00:01:00 7 August and 00:00:00 8 August. Background is a TRI intensity image acquired on 6 August 2012. (**c**), LOS velocity time series between 6 August and 10 August (dots between two grey lines in (a)). Solid blue curve shows the best fit after "apparent outliers" (defined by modified Z-score method) removed, by using a 2nd-order polynomial + 3 pairs of sinusoids model. Dashed blue curves show 3 times RMS space of the residuals. Solid and dashed Light blue curves are blue curves moved upwards/downwards by integer numbers of radar wavelength cycle. Dots fall into the 3×RMS spaces (red) were used in (d), grey dots were removed as outliers. (**d**), Time series from (c) after shifting upwards by phase jump of 4 cycles of radar wavelength, and applying a median filter with a window-size of 3 (equals to 9 min in this case, where the repeating time of measurement is 3 min). Upper blue curve shows the best fitting by the same model as (c), but used filtered time series. Lower blue curves show the 2nd-order polynomial and sinusoids components, offset by some random values. Cyan curve shows local tidal height rate prediction.

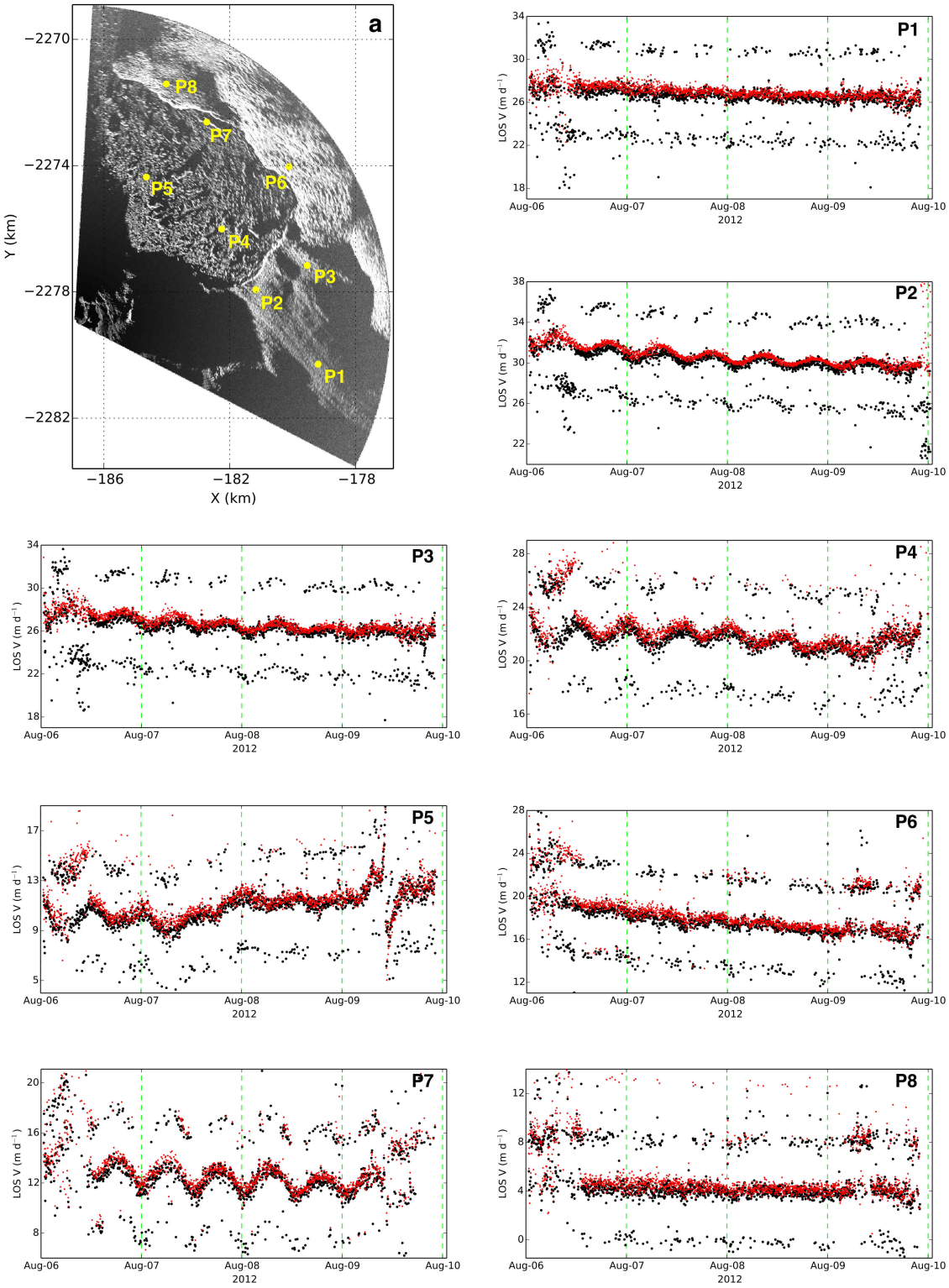

Figure S2. LOS velocities for selected points, after phase jumps fixed. (**a**), Point locations for P1 - P8. (**P1-P8**), Red dots are phase jumps fixed time series, black dots are time series when choosing a stationary point as reference for phase unwrapping, and were shifted upwards by 4 cycles of phase jumps.

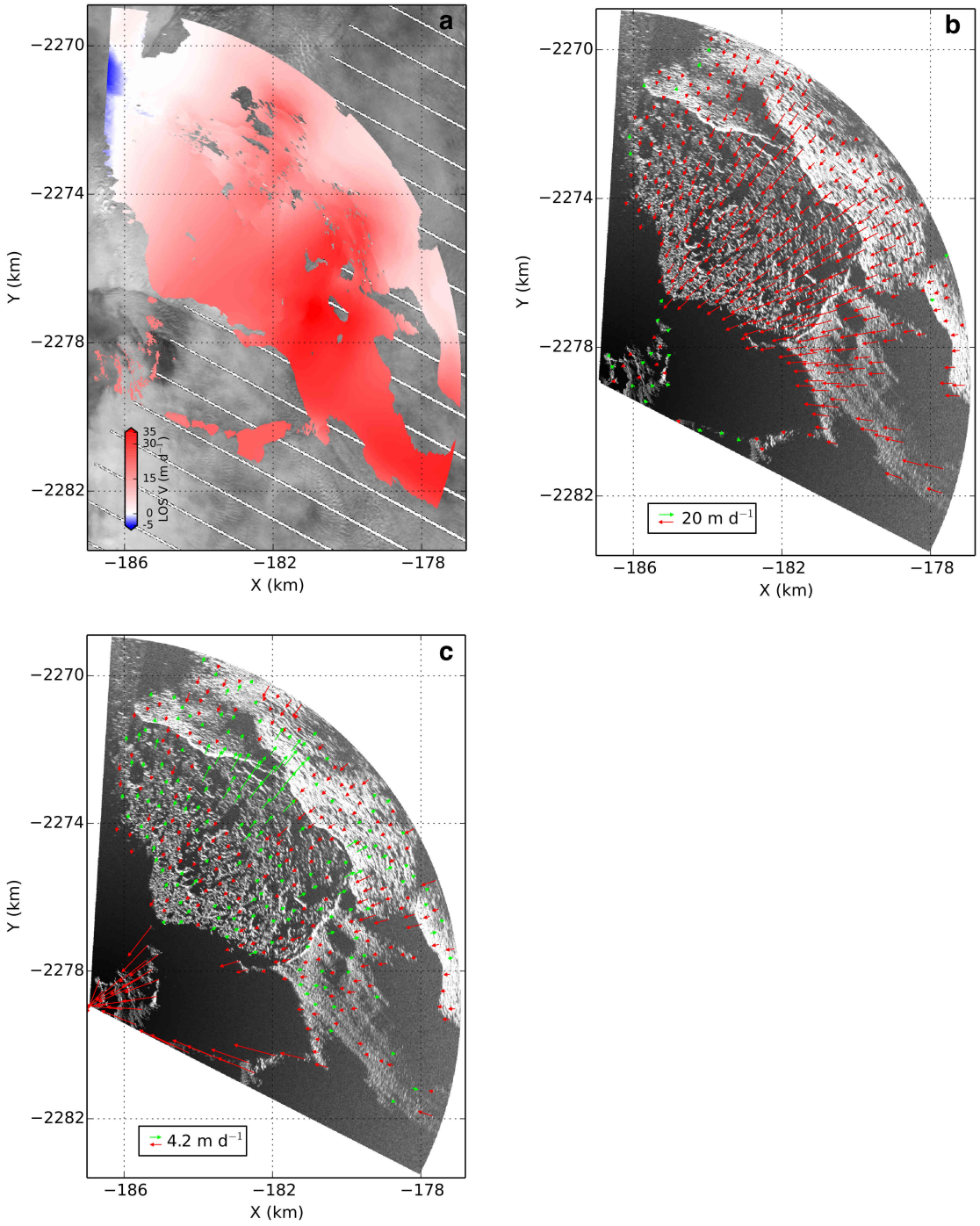

Figure S3. Comparison between velocity estimated by interferometry and feature tracking. (**a**), Median LOS velocity map by interferometry method for 7 August 2012, after phase jump fixed. Background is a Landsat-7 image acquired on 6 August 2012, white stripes are data gaps. (**b**), Velocity map by feature tracking method, projected onto radar LOS direction. Red moves towards the radar, green away. (**c**), Difference between (a) and (b), red when velocity by interferometry is larger than by feature tracking, blue vise versa. 4.2 m d^{-1} equals to 1 cycle of phase jump.

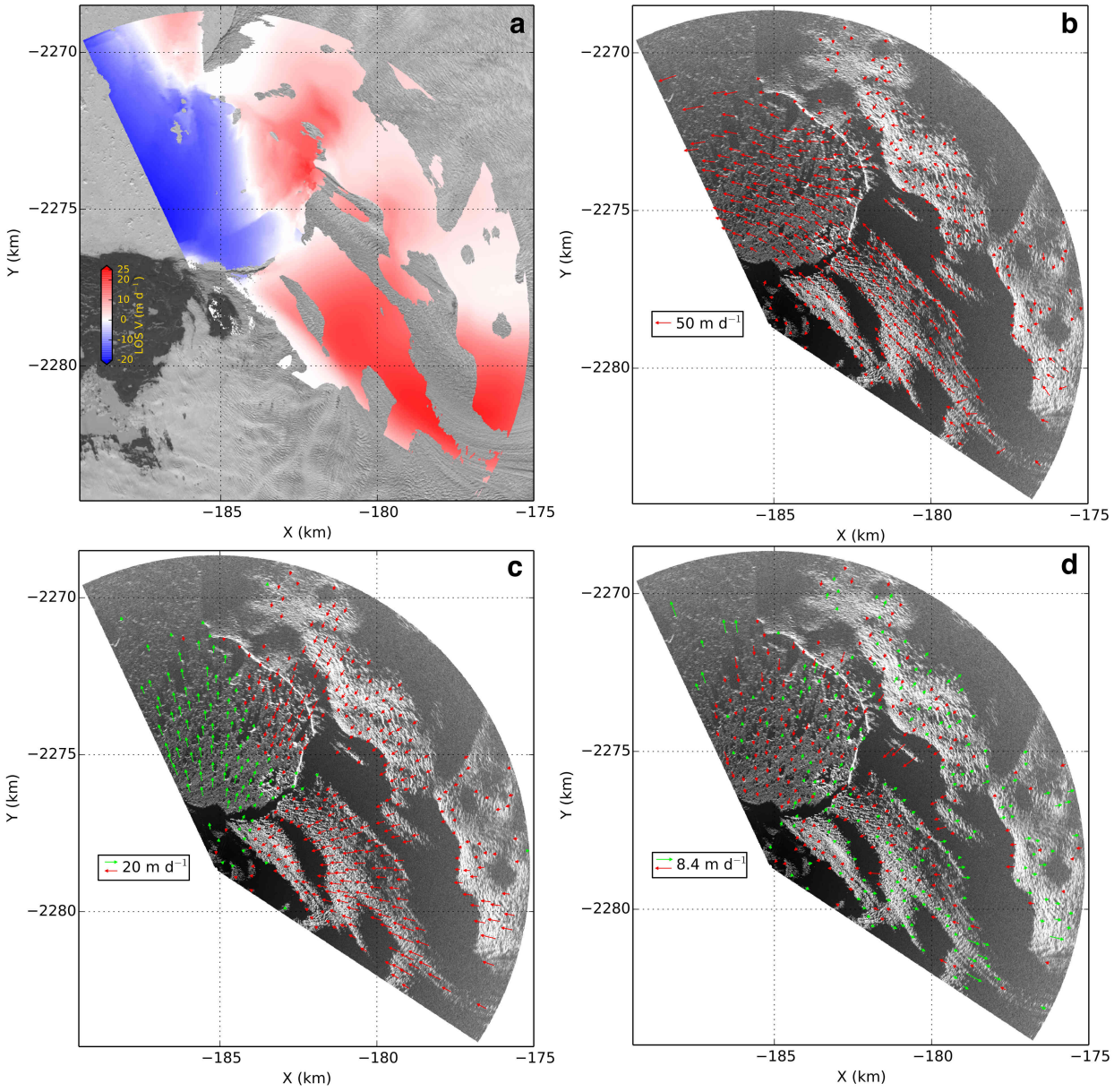

Figure S4. Comparison between velocity estimated by interferometry and feature tracking in 2015. (**a**), LOS velocity map by interferometry. (**b**), 2-D velocity map by feature tracking. (**c**), Velocity map by feature tracking method, projected onto radar LOS direction. Red moves towards the radar, green away. (**d**), Difference between (a) and (c), red when velocity by interferometry is larger than by feature tracking, blue vise versa. 8.4 m d^{-1} equals to 1 cycle of phase jump, when repeating time was 1.5 min.

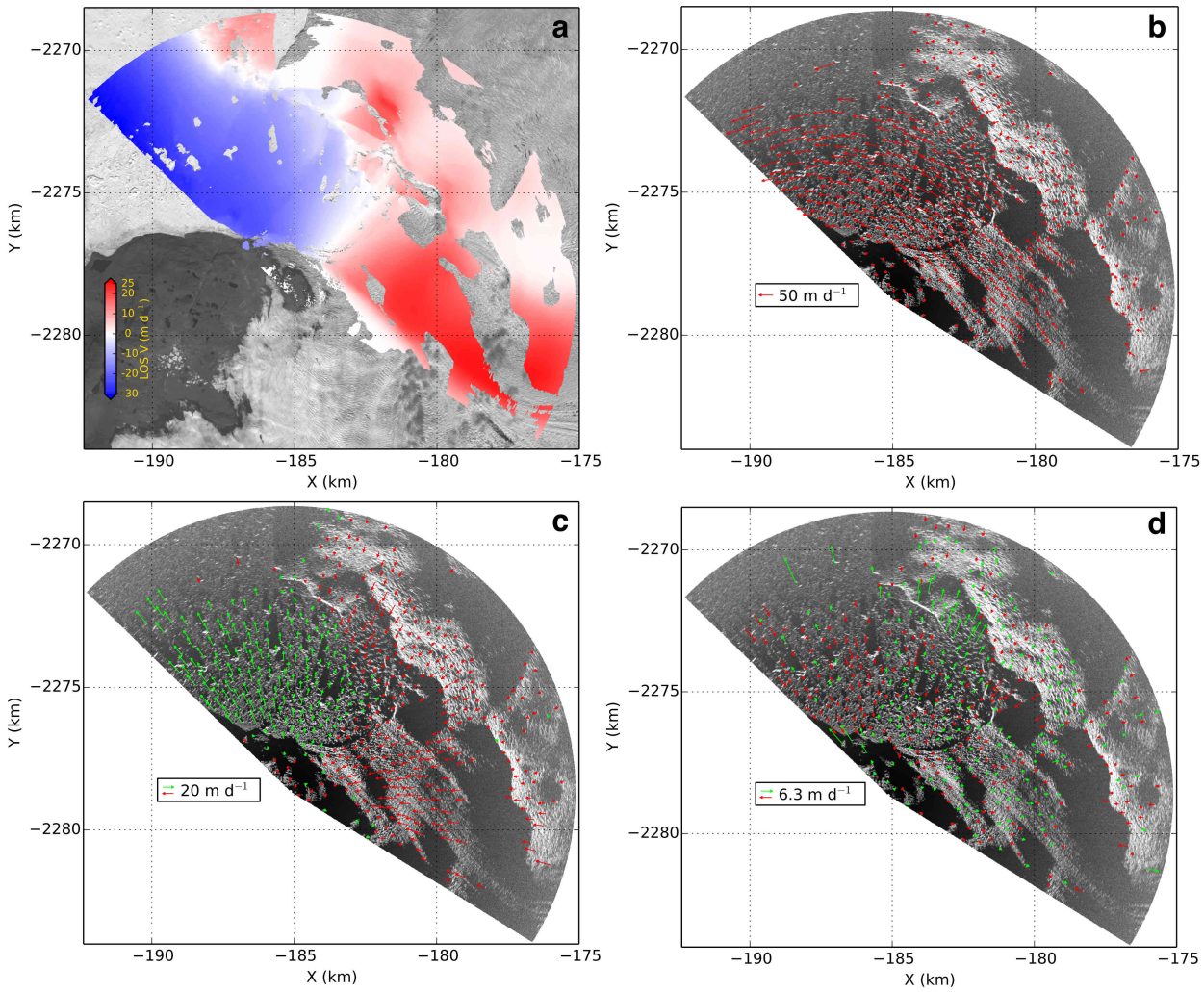

Figure S5. Comparison between velocity estimated by interferometry and feature tracking in 2016. Color and arrow denote the same as Fig. S4. In (d), 6.3 m d^{-1} equals to 1 cycle of phase jump, when repeating time was 2 min.

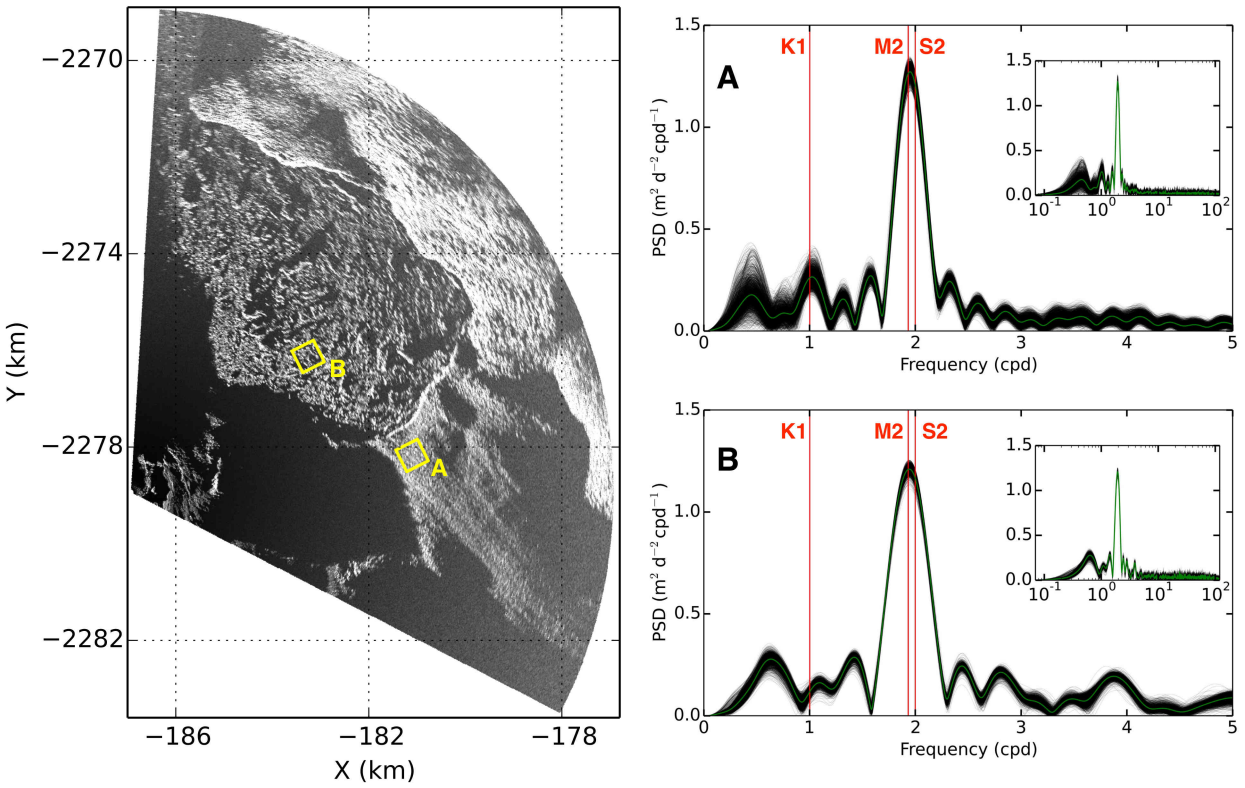

Figure S6. Stacked power spectral density (PSD) estimates of the LOS velocity time series for selected areas in 2012. Two 0.5 km × 0.5 km boxes (A and B) mark the selected areas. For PSD plots, each black line represents 1 pixel (10 m × 10 m) in the corresponding box. Dark green show the mean value. PSDs shown here are normalized. Inserted figures show a wider range of frequency. PSD analysis was done by using the Lomb-Scargle method (Lomb, 1976; Scargle, 1982). Red lines mark the frequencies of K1, M2, and S2 tide constituents.

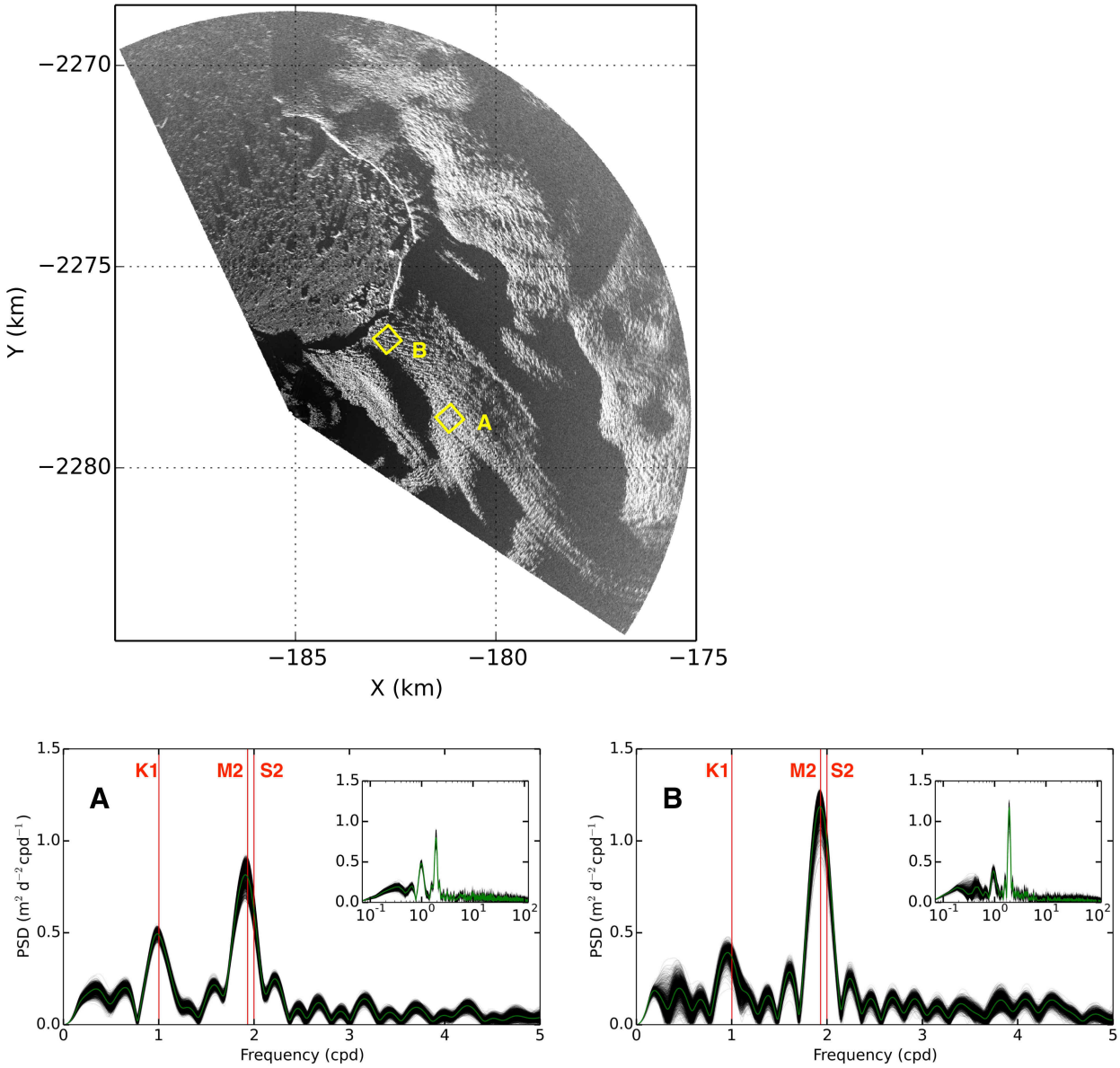

Figure S7. PSD plot for selected samples in 2015. Lines and colors denote the same as in Fig. S6.

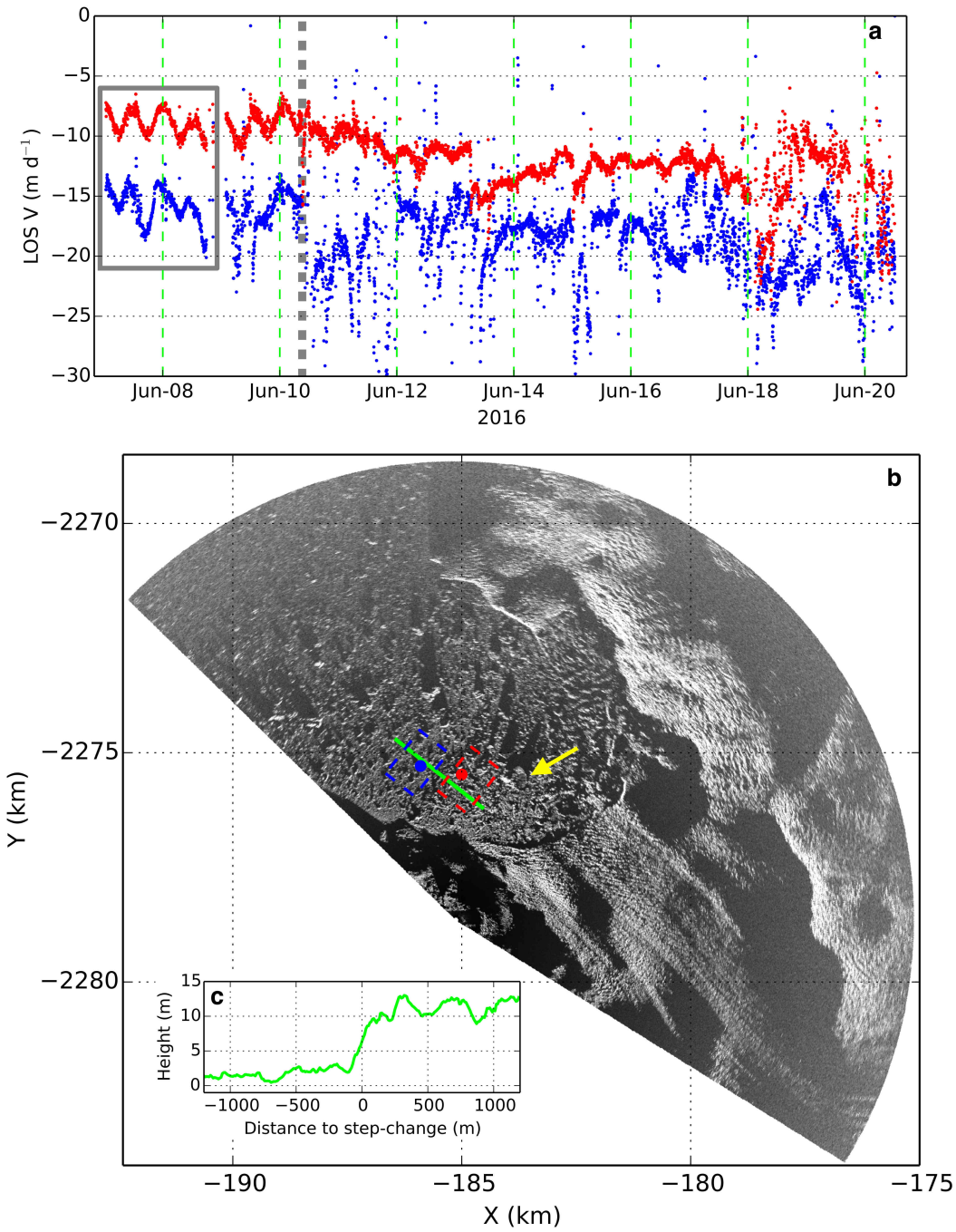

Figure S8. LOS velocity time series for points upstream and downstream from the step-change line. (**a**), Red and blue time series correspond to points in (b) with the same color. Dashed grey line mark the first major calving events observed by TRI. Grey box outlines time series where two ice points move in phase with each other. (**b**), TRI intensity image acquired on 13 Jun 2016. Two dashed boxes were used to derive height difference across the step-change zone. Yellow arrow marks the iceberg with surface elevation ~60 m above local sea level. Green line marks a transect across the step-change, the height profile is in (c). (**c**), Elevation profile of the transect.

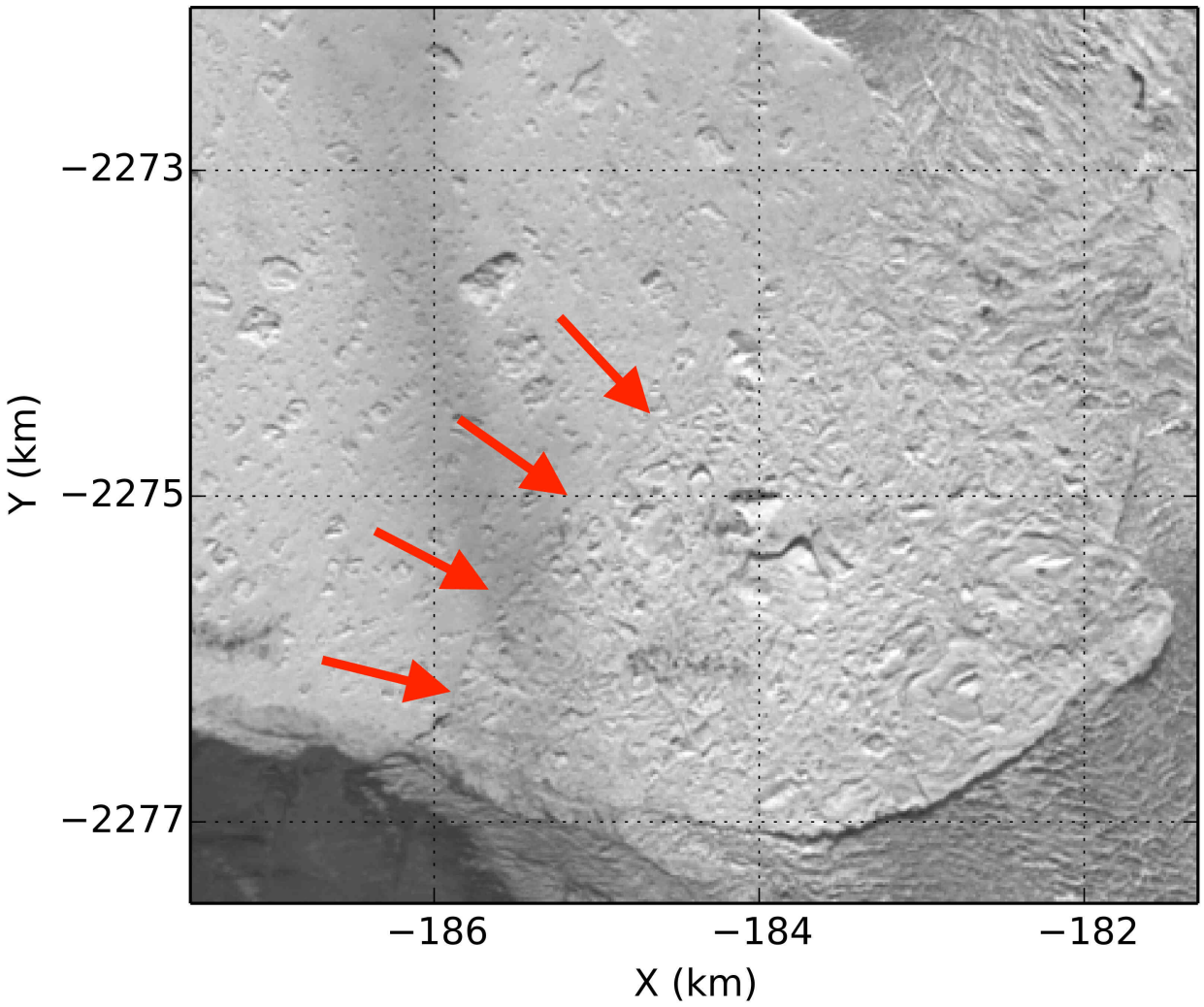

Figure S9. Difference in surface roughness across the step-change. Red arrows mark the step-change shown on a Landsat-8 image acquired on 13 Aug 2016.

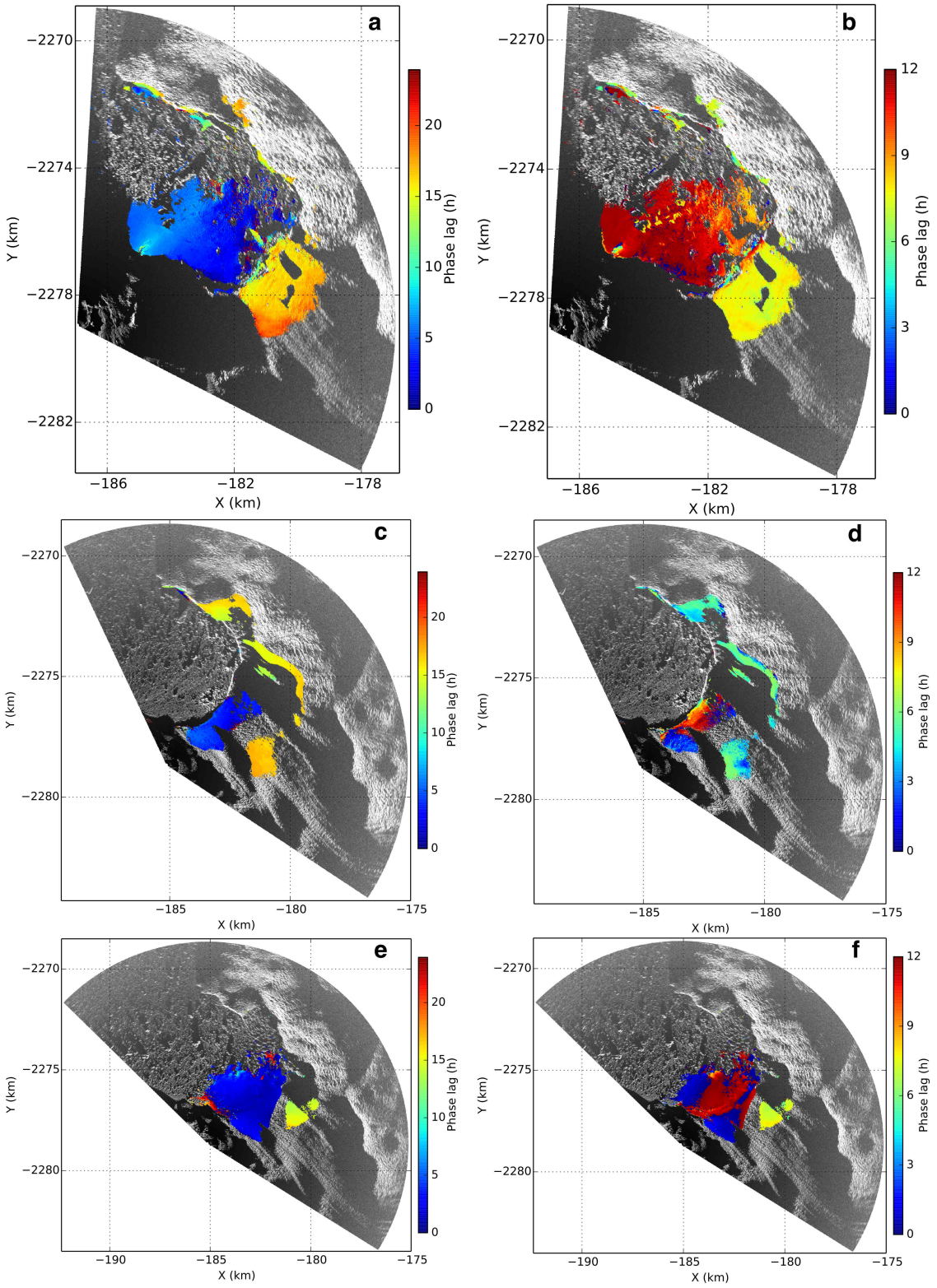

Figure S10. Phase lag maps of signals with K1 and S2 frequencies for each campaign. (a-b) for 2012, (c-d) for 2015, (e-f) for 2016. (a, c, e) show phase lags in time (h) for K1 frequency signal. (b, d, f) for S2 frequency signal. areas where SNR<1.5 are omitted.